Tensile deformation of polytetrafluoroethylene hollow fiber membranes used for water purification

Akio Yonezu, Shouichi Iio, Takehiro Itonaga, Hiroshi Yamamura and Xi Chen

ABSTRACT

The tensile deformation behavior of polytetrafluoroethylene (PTFE) hollow fiber membranes is studied. PTFE membranes at present have sub-micron pores with an open cell structure, which plays a critical role in water purification. One of the main challenges in water purification is that the pore structure becomes covered with biofouling, leading to blocked pores. To maintain the capacity for water purification, physical cleaning along with mechanical deformation is usually conducted. Thus, it is crucial to understand the mechanical properties, in particular the deformation behavior, of the membrane fibers. Using uniaxial tension experiments, we established a fundamental discrete model to describe the deformation behavior of a porous structure using a finite element method. The present model enables the prediction of the macroscopic deformation behavior of the membrane, by taking into account the changes of pore structure. The insight may be useful for porous membrane fabrication and provide insights for the reliable operation of water purification.

Key words | finite element method, hollow fiber membranes, mechanical property, porous polymer material, tensile deformation

Akio Yonezu (corresponding author)
Shouichi Iio
Takehiro Itonaga
Department of Precision Mechanics,
Chuo University,
1-13-27 Kasuga, Bunkyo, Tokyo 112-8551,
Japan
E-mail: *yonezu@mech.chuo-u.ac.jp*

Hiroshi Yamamura
Department of Integrated Science and Engineering for Sustainable Society,
Chuo University,
1-13-27 Kasuga, Bunkyo, Tokyo 112-8551,
Japan

Xi Chen
Department of Earth and Environmental Engineering,
Columbia University,
500 W 120th Street, New York, NY 10027,
USA
and
International Center for Applied Mechanics,
SV Lab, School of Aerospace, Xi'an Jiaotong University, Xi'an 710049,
China

INTRODUCTION

Membrane filtration is a promising technology in drinking and wastewater treatment, because it strictly removes suspended solids without any chemical addition (Shannon *et al.* 2008). The configuration of polymeric membranes for water treatment is roughly classified into flat sheet, hollow fiber, and tubular types. With the advance of high packing density, hollow fiber membrane is often selected for water purification processes (Mulder 1996; Tang *et al.* 2012). The major drawback of membrane filtration is membrane fouling, and it still remains a major obstacle for efficient use of the membrane process. In practice, membrane fouling is mitigated by physical or chemical cleaning. Physical cleaning including air scrubbing or backwashing is routinely applied in place and removes the contaminants accumulating on the surface of the membrane. The efficiency of physical cleaning is strongly dependent on the cleaning conditions (such as frequency and amplitude of fiber movement), i.e. the more the fibers are moving the more foulants are moved away (Matsumoto *et al.* 1996). Although thin and slim fiber is easily moved with wide amplitude and high frequency, such fiber is easily fractured, where the repeated physical cleaning leads to shortening of the membrane lifetime. To achieve both physical strength and cleaning efficiency, we need to optimize the macroscopic and microscopic dimensions of the fiber on the basis of the deeper understanding of the mechanical properties of hollow fiber membranes. However, there is still a lack of information on the relationship between porous structure and mechanical characteristics (i.e. macroscopic deformation and fracture strength of entire fiber membranes).

Most commercial hollow fiber membranes are now fabricated by phase inversion or stretching methods (Mulder 1996). The stretching method, mechanically stretching a crystalline polymer below the melting point to locally break the non-crystalline part, is often prepared with polyethylene (Mulder 1996). Although the stretching method provides relatively good mechanical properties due to aligned molecular chains, the inherent pore structure has inferior macroscopic mechanical properties compared

doi: 10.2166/wst.2014.364

with 'solid' counterparts (matrix materials). Previous studies have attempted to improve mechanical properties in terms of tensile loading. For example, clay, different polymer particles and carbon nanotubes were incorporated into a polymer matrix to create a reinforced mixed matrix structure (Teoh & Chung 2009; Wang *et al.* 2009; Su *et al.* 2010). Recently, polytetrafluoroethylene (PTFE) membrane has been developed by a manufacturer and shows excellent chemical resistance (Sumitomo Electric Fine Polymer, Inc.; Wan *et al.* 2012). In addition, several studies have reported the use of PTFE membrane for the treatment of chemical wastewater (Hu & Scott 2008; Lee *et al.* 2012). In parallel, numerical simulation has been attempted to optimize the fabrication process of hollow fiber membrane (Yang *et al.* 2006), and understand the deformation behavior (Lee & Youn 2006).

To improve the physical property of the PTFE membrane, this study investigated the deformation behavior of PTFE hollow fiber membrane under uniaxial tensile loading. Tensile tests with various strain rates were carried out to clarify the mechanical deformation behavior (i.e. stress–strain curve), including yield stress and tensile strength. Based on the experimental results, we propose the fundamental mechanics of deformation behavior, using a finite element method (FEM) on porous structure. The predictive model may be useful for designing material structures for a given polymer and porosity. The present study shed some light on pore-structure design for physical cleaning as well as for reliability in water purification.

MATERIALS AND EXPERIMENTAL SETUP

The material used in this study is hollow fiber membrane for water purification (Sumitomo Electric Industry Ltd, Osaka, Japan). For the sample configuration, the outer diameter was 2.43 mm and inner one was 1.14 mm. The wall thickness was about 0.65 mm. This is commercially available as a module component for water purification. PTFE of crystalline polymer was stretched to create a sub-micron pore structure. As discussed later, the structure showed random network and open cell structure. The overall porosity was estimated to be 75% based on the density measurement. In that measurement, the volume of the fiber membrane was calculated according to the inner/outer diameters and the fiber length. Note that the density of intrinsic PTFE is 2.13–2.2 g/cm^3.

Uniaxial tensile tests were performed using a universal testing machine with ball screw type (LSC-1/30: Tokyo Testing Machine Inc.). The membrane fiber was wound on the testing fixture, so that it applied uniform tensile stress to the fiber membrane. The clamp distance, corresponding to a gage length, was about 195 mm. The tests were conducted under displacement control with the different strain rates of 8.55×10^{-5}, 4.27×10^{-4}, and 2.56×10^{-3} s^{-1} at room temperature. For each test, the average data of at least three measurements were taken.

EXPERIMENTAL RESULTS

As shown in Figure 1, the outer surface of the membrane was observed by scanning electron microscope (SEM, Qunta 250, FEI Corp.) (Figure 1(a)) and atomic force microscope (AFM, E-sweep, Hitachi High-Tech Corp.) (Figure 1(b)). It was found that the membrane under study had an open-cell porous structure. Note that the arrows indicate the longitudinal direction of the specimen. The pore shape is stretched elliptically and the direction of the longer axis coincides with the longitudinal direction of the hollow membrane. From the observations of Figure 1, the pore size and shape were measured. The pore size as a true circular shape

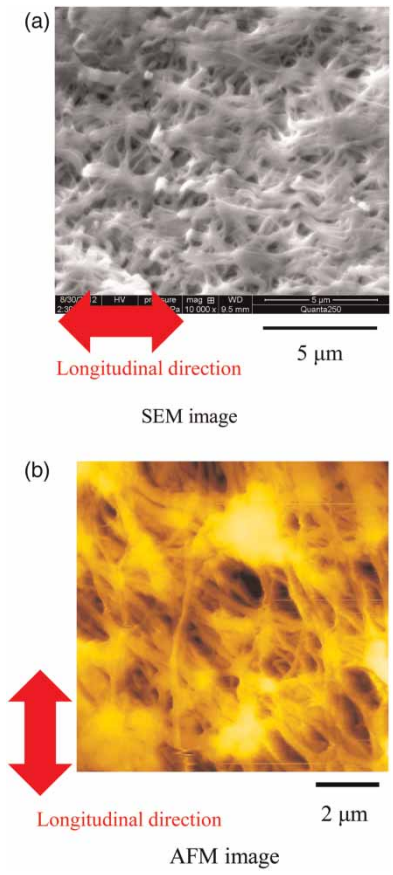

Figure 1 | Microstructure of hollow fiber membrane.

was roughly estimated to be in the range from 0.1 to 1 μm, and the averaged value was 0.5 μm. Subsequently, we measured the pore shape, i.e. elliptical pore axis ratio (the length ratio of short and long axes). This ranged between 1.5 and 4 with an average value of 3.

Figure 2 shows the nominal stress–strain curve of each test with different strain rates. With the increase in tensile strain, the nominal stress increased gradually and reached a maximum stress. Subsequently, the stress value was almost constant. This is called the 'plateau' region. The maximum peak stress (plateau stress) strongly depended on the strain rate $\dot{\varepsilon}$. Finally, it reached the final fracture as indicated by 'x' in this figure.

We next investigated how the fiber membrane deformed elastically and plastically. In this study, loading and unloading tests were carried out as shown in Figure 3. At a certain tensile load, the loading was stopped and released down to zero. (In fact, after the loading was reduced to zero, the specimen was unfixed from the jig: the bottom of the membrane specimen was unclamped from the jig, such that the specimen was in a completely unloaded condition (no-loading condition). This test measured the strain in a non-contact manner using a video camera.) Several tests with different peak loads were conducted. For all tests, the strain rate was set to $4.27 \times 10^{-4}\ s^{-1}$. As shown in Figure 3, the peak loads were chosen to be (A) ($\sigma = 1.51$ MPa, $\varepsilon = 0.034$), (B) ($\sigma = 9.99$ MPa, $\varepsilon = 0.13$), (C) ($\sigma = 15.0$ MPa, $\varepsilon = 0.15$), (D) ($\sigma = 18.0$ MPa, $\varepsilon = 0.29$) and (E) ($\sigma = 18.2$ MPa, $\varepsilon = 0.45$). It was found that the unloading curve did not match with loading one, indicating that the deformation behavior

Strain rate	Test num
8.55×10^{-5}	4
4.27×10^{-4}	3
2.56×10^{-3}	5

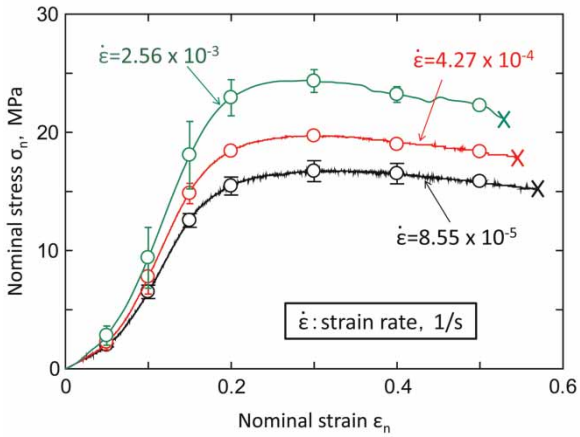

Figure 2 | Experimental nominal stress–strain curves at different strain rates.

	○(A)	△(B)	▽(C)	□(D)	◇(E)
σ_n, MPa	1.51	9.99	15.00	18.04	18.20
ε_n	0.034	0.13	0.15	0.29	0.45

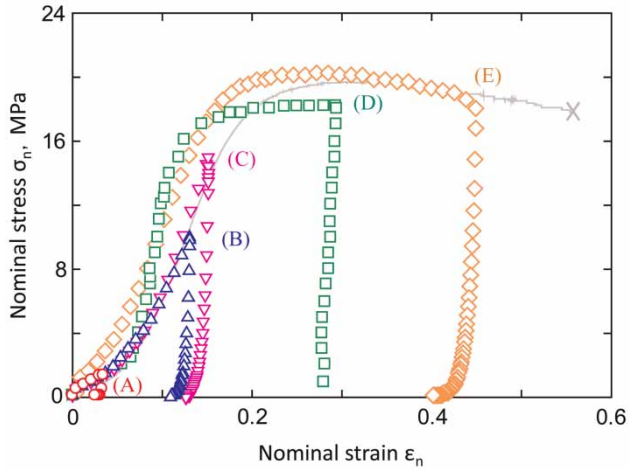

Figure 3 | Nominal stress–strain curves of repeated loading–unloading tests.

under study had a hysteresis loop. After complete unloading, we carefully observed the changes in total strain. The result plotted in Figure 4(a) shows the strain history after complete unloading (i.e. the specimen was left in a no-loading state for up to 2,880 min (2 days)). For all tests, the strain decreased with the test time, and became a constant value. This is the time-dependent behavior (like viscoelastic recovery). However, the plateau of the total strain (after a long period of being left) was different for each test, and was dependent on the applied stress (or strain) designated by (A–E). For the (A), (B) and (C) tests, the strain gradually recovered back to the initial state (almost no plastic strain). However, tests (D) and (E) showed that the strain did not recover completely. Therefore, those strain values (i.e. the remaining plastic strain after complete recovery) were next investigated as shown in Figure 4(b). As expected, (A), (B) and (C) tests showed no plastic strain, indicating that they recovered completely. However, (D) and (E) tests retained the plastic strain. This means that the specimen in (D) and (E) underwent plastic deformation, retaining the plastic strain.

With these results (Figure 4(b)) compared with Figure 3, the regions of elastic and plastic deformation were explored. Tests (A), (B) and (C) (before reaching the maximum peak stress) showed elastic deformation (i.e. complete recovery upon unloading). By contrast, tests (D) and (E), which reached the plateau region, produced plastic strain. Therefore, it can be concluded that the specimen first deformed elastically, and then developed a plateau due to macroscopic plastic deformation. Such a unique behavior may be caused

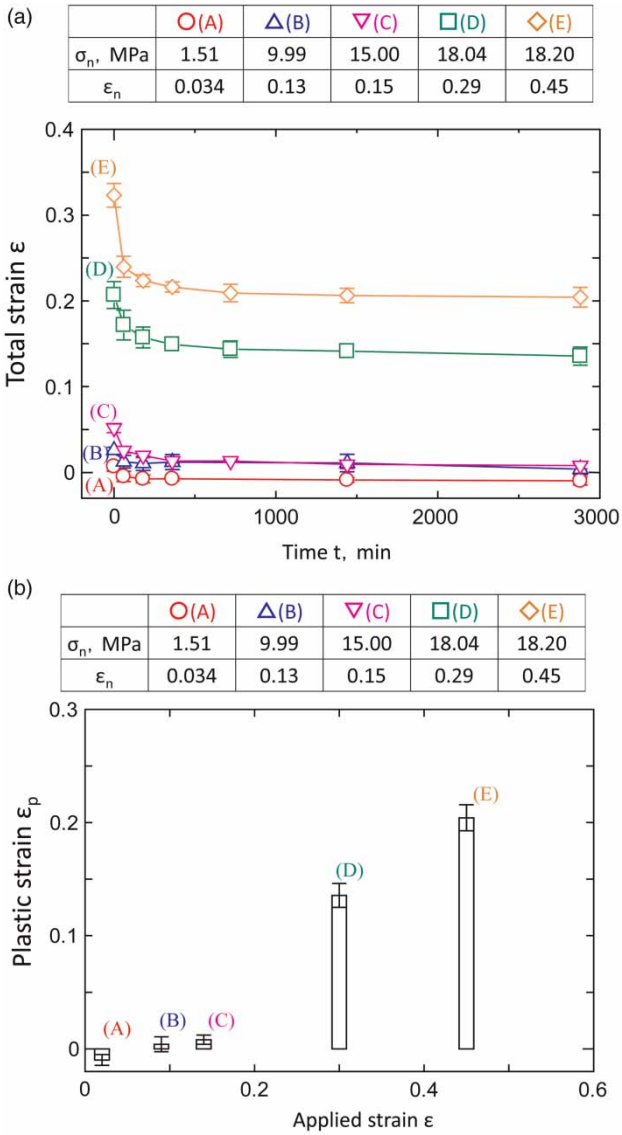

Figure 4 | Changes in (a) total strain as a function of time after unloading and (b) plastic strain with respect to the applied strain.

by an inherent pore structure as well as the property of the PTFE matrix.

To establish the computational approach for describing macroscopic deformation of the membrane under study, FEM incorporating pore structure was employed as described in the next section.

DISCUSSION

As discussed above, the macroscopic deformation depends on the elastoplastic properties of the PTFE matrix and inherent porous structure. Thus, a FEM model was created including pore structure (described in the next section). Next, we explored the agreement between the computed stress–strain curve and the experimental one. In this process, both elastic analysis and elastoplastic analysis were conducted, so as to exemplify the material constant in the constitutive equation of the PTFE matrix (described in the section 'Deformation behavior').

Finite element simulation

Figure 5 shows the FEM model of the hollow fiber membrane under study. As mentioned above, the porosity of the membrane was 75%. For the representative element of pore structure, the effective pore diameter (as if the pore were circular) was 0.5 μm (the area was about 0.15 μm^2), and the aspect ratio was about 3. The representative element structure of the FEM model is given in Figure 5. For simplicity, the pore shape was assumed to be semi-periodic along the longitudinal direction. A mesh converge test was carried out and frictionless contact was modeled at the edge line of the pore.

As shown in Figure 5(b), the left end of the specimen was fixed, and the right end was extended by a uniaxial tensile load. The plane stress condition was assumed for the present two-dimensional model. At the right end, the longitudinal displacement and reaction force were computed, in order to obtain the nominal stress and strain curve, and compare with the experimental stress–strain curve.

As discussed for Figures 3 and 4, elastic and plastic deformation regions were observed. Thus, the present study conducted (1) elastic analysis and (2) elastoplastic analysis, respectively. We employed elastic parameters whereby Young's modulus of the PTFE matrix E was 580 MPa and Poisson's ratio ν was 0.4 (Rae & Brown 2005). For the plastic property, several constitutive equations for polymers have been developed in previous studies; among them, the following simple phenomenological equation can be applied for large tensile strain (Nunes *et al.* 2011):

$$\sigma = \sigma_Y + K(\varepsilon)^m \tag{1}$$

Here, σ_Y is the yield stress, K and m are the materials constants to describe the nonlinear plastic deformation and ε is the plastic strain. Nunes *et al.* (2011) reported that when the tensile load was applied to PTFE solid material, σ_Y was dependent on the strain rate $\dot{\varepsilon}$, while K and m

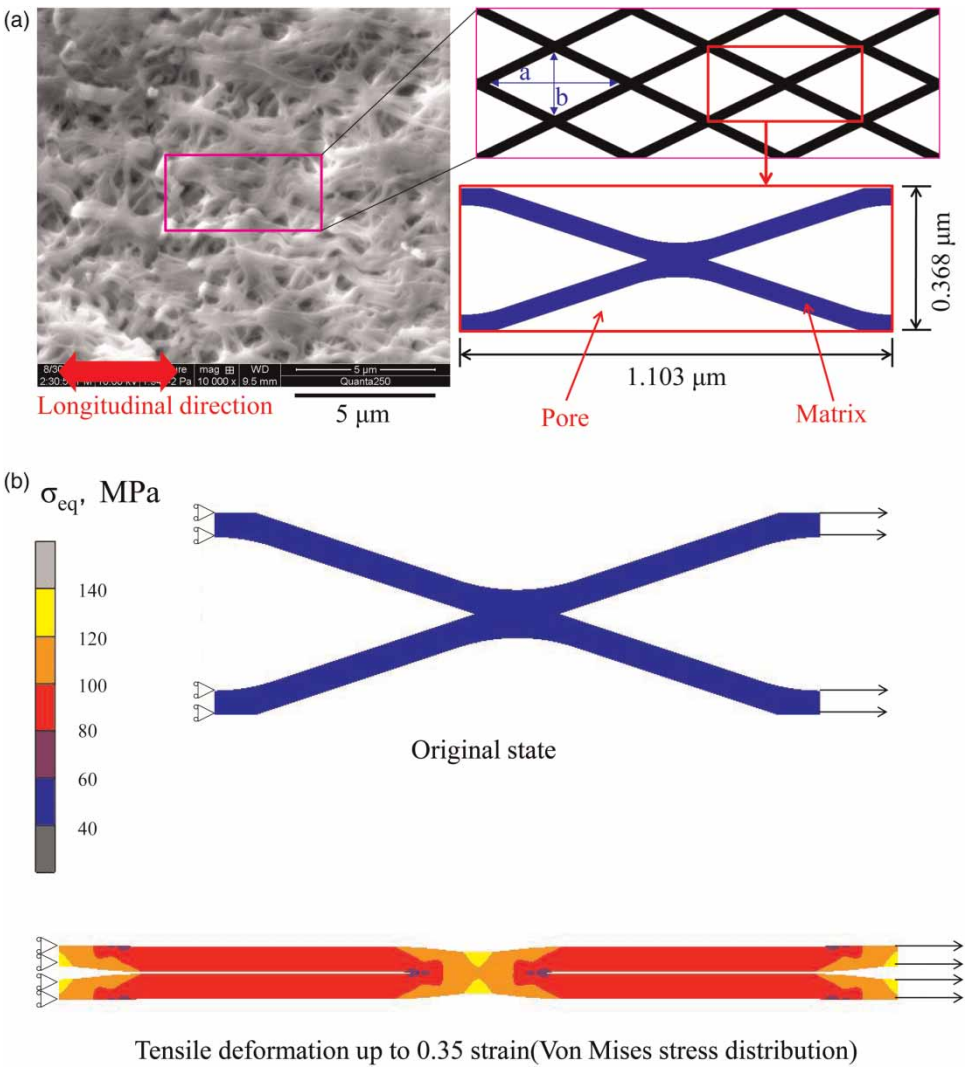

Figure 5 | (a) Simplified FEM model of porous structure and (b) FEM model with boundary condition and the contour map of stress distribution at 0.35 strain.

were independent of $\dot{\varepsilon}$. (The constitutive law of Equation (1) does not include strain rate dependency. According to Nunes *et al.* (2011), the strain rate dependency appears in material constants in Equation (1). Thus, the present study investigated the constants for each strain rate.) However, the material constants (σ_Y, K and m in Equation (1) for the PTFE matrix) were unclear in this study. This is due to the changes in matrix microstructure (such as aligned molecular chains), since the PTFE matrix was significantly stretched in order to create the porous structure. Such a fabrication method seems to induce a work-hardened nature. In order to estimate the properties, the computed stress–strain curve was matched with the experimental one by repeatedly changing the material constants (σ_Y, K and m) of the constituent material in Equation (1).

Deformation behavior

Figure 6 shows the stress–strain curve from the experiment (the same as Figure 2) and the computational one. The computed result (as shown by open circle marks) was obtained by elastic analysis, where it is governed by Hook's law ($\sigma = E\ \varepsilon$). Similar to the experimental data, the FEM result also showed nonlinear deformation in the first portion, owing to the structural deformation of pore geometry. After the nonlinear deformation, the stress linearly increased up to the maximum stress. The stress-increasing part showed relatively good agreement with experimental curves.

We next investigated the plastic deformation with elastoplastic analysis, using Equation (1) to describe the plastic deformation. As shown in Figure 2, the plastic

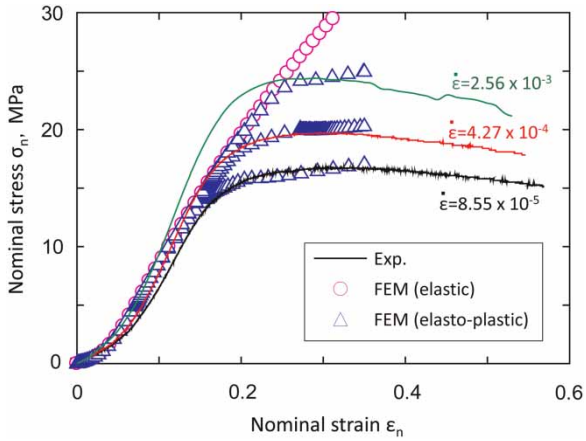

Figure 6 | Nominal stress–strain curve from experiment and FEM (circle mark: elastic analysis, triangle mark: elastoplastic analysis). The experimental data are obtained from Figure 2.

deformation (at the maximum stress in the plateau region) is strongly dependent on the strain rate $\dot{\varepsilon}$. Thus, we calibrated the material parameters in the FEM model such that they might deduce a similar strain rate effect to that measured in experimental stress–strain curves. In order to match the FEM analysis with experimental ones, the material constants (σ_Y, K and m in Equation (1)) were optimized at given strain rates through error minimization.

As shown by the triangle marks (in Figure 6), all tests indicated a good agreement when the proper material constants were selected. (Note that the simulation was terminated when the strain reached about 0.35, since a larger strain might have induced fiber fracture, pore growth and coalescence. Such a fracture effect is not included in this FEM model.) Similar to the experimental data, the computed result showed that the nominal stress became nonlinear with increasing strain, and developed a plateau region. From this parametric FEM study, the material constants of Equation (1) were obtained as follows. The yield stresses σ_Y for the test of $\dot{\varepsilon} = 8.55 \times 10^{-5}$, 4.27×10^{-4} and $2.56 \times 10^{-3}\,\mathrm{s}^{-1}$ were estimated to be 65, 85 and 115 MPa, respectively. The relationship between σ_Y and $\dot{\varepsilon}$ was fitted as

$$\sigma_Y = 14.75 \ln(\dot{\varepsilon}) + 201.9 \quad (2)$$

By contrast, the constants K and m were 330 MPa and 1.4, which were independent of $\dot{\varepsilon}$. The constants (σ_Y, K and m) correspond to a parameter of the PTFE fiber matrix. This trend is similar to that of PTFE as a solid material (Nunes *et al.* 2011). It is noted that the bottom of Figure 5(b) shows an inhomogeneous stress distribution, suggesting that the strain and strain rate are not uniform during the uniaxial tension. When a constitutive law with strain rate effect (e.g. the G'sell-Jonas law (G'Sell & Jonas 1979)) is employed in the FEM, we can develop a more accurate mechanical model.

CONCLUSION

This study proposed a simple model to predict the tensile deformation behavior of PTFE hollow fiber membranes. During water purification, it is often necessary to apply mechanical deformation (physical cleaning) to remove biofouling covering the membrane surface. The mechanical framework developed herein is useful for understanding the fundamental mechanical behavior and ensuring the integrity of the membrane.

This study first investigated the deformation behavior of an entire fiber membrane using uniaxial tensile experiments. The specimen deformed elastically and plastically, at small and large strains, respectively. During the plastic deformation, a plateau region in the stress–strain curve was observed, which corresponded to the maximum nominal stress (i.e. tensile strength), and also strongly depended on the strain rate.

Based on the experimental results, we established a mechanical model and simulated the overall behavior using FEM, incorporating the pore structure measured by SEM and AFM. A parametric FEM study was conducted to extract the rate-dependent material constants of the constitutive equation of the PTFE matrix. This model enable the prediction of macroscopic tensile deformation behavior, at different strain rates.

ACKNOWLEDGMENTS

The work of A.Y. was supported in part by JSPS KAKENHI (grant no. 26420025) and JGC-S Scholarship Foundation. The work of X.C. is supported by the National Natural Science Foundation of China (grant nos. 11172231 and 11372241), AFOSR (FA9550-12-1-0159), and DARPA (W91CRB-11-C-0112).

REFERENCES

G'Sell, C. & Jonas, J. J. 1979 Determination of the plastic behaviour of solid polymers at constant true strain rate. *Journal of Materials Science* **14**, 583–591.

Hu, B. & Scott, K. 2008 Microfiltration of water in oil emulsions and evaluation of fouling mechanism. *Chemical Engineering Journal* **136**, 210–220.

Lee, E. S. & Youn, S. K. 2006 Finite element analysis of wrinkling membrane structures with large deformations. *Finite Elements in Analysis and Design* **42**, 780–791.

Lee, E. J., Kim, K. Y., Lee, Y. S., Nam, J. W., Lee, Y. S., Kim, H. S. & Jang, A. 2012 A study on the high-flux MBR system using PTFE flat sheet membranes with chemical backwashing. *Desalination* **306**, 35–40.

Matsumoto, Y., Miwa, T., Nakao, S. & Kimura, S. 1996 Improvement of membrane permeation performance by ultrasonic microfiltration. *Journal of Chemical Engineering of Japan* **29**, 561–567.

Mulder, J. 1996 *Basic Principles of Membrane Technology*. 2nd edn, Kluwer Academic Publishers, Dordrecht, The Netherlands.

Nunes, L. C. S., Dias, F. W. R. & Mattos, H. S. d. C. 2011 Mechanical behavior of polytetrafluoroethylene in tensile loading under different strain rates. *Polymer Testing* **30**, 791–796.

Rae, P. J. & Brown, E. N. 2005 The properties of poly (tetrafluoroethylene) (PTFE) in tension. *Polymer* **46**, 8128–8140.

Shannon, M. A., Bohn, P. W., Elimelech, M., Georgiadis, J. G., Marinas, B. J. & Mayes, A. M. 2008 Science and technology for water purification in the coming decades. *Nature* **452**, 301–310.

Su, M., Teoh, M. M., Wang, K. Y., Su, J. & Chung, T.-S. 2010 Effect of inner-layer thermal conductivity on flux enhancement of dual-layer hollow fiber membranes in direct contact membrane distillation. *Journal of Membrane Science* **364**, 2478–2289.

Sumitomo Electric Fine Polymer, Inc. POREFLON™ MEMBRANE, http://www.sei-sfp.co.jp/english/products/poreflon-membrane.html.

Tang, Y., Li, N., Liu, A., Ding, S., Yi, C. & Liu, H. 2012 Effect of spinning conditions on the structure and performance of hydrophobic PVDF hollow fiber membranes for membrane distillation. *Desalination* **287**, 326–339.

Teoh, M. M. & Chung, T. S. 2009 Membrane distillation with hydrophobic macrovoid-free PVDF–PTFE hollow fiber membranes. *Separation and Purification Technology* **66**, 229–236.

Wan, M. W., Yang, H. L., Chang, C. H., Reguyal, F. & Kan, C. C. 2012 Fouling elimination of PTFE membrane under precoagulation process combined with ultrasound irradiation. *American Society of Civil Engineers* **138**, 337–343.

Wang, K. Y., Foo, S. W. & Chung, T. S. 2009 Mixed matrix PVDF hollow fiber membranes with nanoscale pores for desalination through direct contact membrane distillation. *Industrial and Engineering Chemistry Research* **48**, 4474–4483.

Yang, X.-T., Xu, Z.-L. & Wei, Y.-M. 2006 Two-dimensional simulation of hollow fiber membrane fabricated by phase inversion method. *Journal of Applied Polymer Science* **100**, 2067–2074.

First received 13 June 2014; accepted in revised form 7 August 2014. Available online 22 August 2014